Shock Propagation Model version 2 and its application in predicting the arrivals at Earth of interplanetary shocks during Solar Cycle 23

X. H. Zhao[1] and X. S. Feng[1]

Received 19 November 2012; revised 21 October 2013; accepted 26 October 2013; published 8 January 2014.

[1] The Shock Propagation Model (SPM) based on an analytic solution of blast waves has been proposed to predict shock arrival times at Earth. Here to reduce the limitations of the SPM theoretical model in real applications and optimize its input parameters, a new version (called SPM2) is presented in order to enhance prediction performance. First, an empirical relationship is established to adjust the initial shock speed, which, as computed from the Type II burst drift rate, often contains observational uncertainties. Second, an additional acceleration/deceleration relation is added to the model to eliminate inherent prediction bias. Third, the propagation direction is derived in order to mitigate the isotropy limitation of blast wave theory in real predictions. Finally, an equivalent shock strength index at the Earth's location to judge whether or not an interplanetary shock will encounter the Earth is implemented in SPM2. The prediction results of SPM2 for 551 solar disturbance events of Solar Cycle 23 demonstrate that the success rate of SPM2 for both shock (W-shock) and nonshock (W/O-shock) events at Earth is $\sim$ 60%. The prediction error for the W-shock events is less than 12 h (root-mean-square) and 10 h (mean-absolute). Comparisons between the predicted results of SPM2 and those of Shock Time of Arrival (STOA), Interplanetary Shock Propagation (ISPM), and Hakamada-Akasofu-Fry version 2 (HAFv.2) based on similar data samples reveal that the SPM2 model offers generally equivalent prediction accuracy and reliability compared to the existing Fearless Forecast models (STOA, ISPM, and HAFv.2).

Citation: Zhao, X. H., and X. S. Feng (2014), Shock Propagation Model version 2 and its application in predicting the arrivals at Earth of interplanetary shocks during Solar Cycle 23, *J. Geophys. Res. Space Physics*, *119*, 1–10, doi:10.1002/2012JA018503.

1. Introduction

[2] Predicting arrival times of interplanetary (IP) shocks at Earth is an important ingredient of space weather forecasting because the passage of an IP shock at Earth will compress the magnetosphere and produce corresponding space weather effects [*Russell et al.*, 2000]. Coronal mass ejections are responsible for producing strong IP shocks. Type II bursts are thought to be the signature of coronal shock waves associated with these solar transients. Both empirical and physics-based models have been proposed to predict shock arrival times (SATs) based on the relationship between features of solar disturbances and their corresponding IP shocks. By using available solar data as input parameters, these physics-based models have been employed to give "near real-time" predictions of shock arrivals at Earth, such as the "Shock Time of Arrival" (STOA) Model [*Dryer and Smart*, 1984; *Smart and Shea*, 1984, 1985], the "Interplanetary Shock Propagation" Model (ISPM) [*Smith and Dryer*, 1990, 1995], and the "Hakamada-Akasofu-Fry version 2" (HAFv.2) model [*Dryer et al.*, 2001, 2004; *Fry et al.*, 2001, 2003, 2007; *McKenna-Lawlor et al.*, 2002, 2006, 2012; *Smith et al.*, 2005, 2009; *Sun et al.*, 2002a, 2002b, 2003]. The STOA, ISPM, and HAFv.2 models use similar input solar parameters, including the source location of the associated flare, the start time of the metric Type II radio burst, the proxy piston-driving time duration, and the background solar wind speed. Their predictions are frequently referred to in the literature as "Fearless Forecasts", and the prediction results were sent to interested members of both scientific and operational communities through emails within 10 h after the solar events. The Fearless Forecast models can predict not only the shock arrival times but also whether or not the IP shock can encounter the Earth by introducing a judgement index (i.e., the Alfvén Mach number in STOA, shock strength index in ISPM, and Shock Searching Index in HAFv.2). There are other physical models established on the base of the Fearless Forecast models. A practical database method for predicting SATs at the L1 point was presented by *Feng et al.* [2009a] based on the HAFv.1 model and a set of hypothetical solar events. STOA was used with the help of solar energetic particle (SEP) observations and/or soft X-ray

Additional supporting information may be found in the online version of this article.

[1]SIGMA Weather Group, State Key Laboratory of Space Weather, Center for Space Science and Applied Research, Chinese Academy of Sciences, Beijing, China.

Corresponding author: X. S. Feng, SIGMA Weather Group, State Key Laboratory of Space Weather, Center for Space Science and Applied Research, Chinese Academy of Sciences, Beijing 100190, China. (fengx@spaceweather.ac.cn)

2169-9380/14/10.1002/2012JA018503

observations at L1 to predict whether a shock will encounter the Earth [*Qin et al.*, 2009; *Liu and Qin*, 2012].

[3] Physics-based magnetohydrodynamic (MHD) numerical models are also often used to provide SAT predictions since they can simulate the propagation of solar disturbances in the background solar wind [*Feng et al.*, 2007, 2011]. *Feng et al.* [2009b] proposed an operational method for SAT prediction using the 1-D Conservation Element and Solution Element (CESE)-Hydrodynamics (HD) solar wind model, and their prediction results demonstrated potential capability of the model to improve real-time forecasting because the CESE method can be extended to three-dimensional (3-D) MHD from the solar photosphere to any heliospheric position [*Feng et al.*, 2007, 2010, 2011, 2012a, 2012b; *Zhou et al.*, 2012]. The 3-D-MHD simulations are promising in real-time space weather predictions. However, they presently need considerable computing resources.

[4] Due to the limitation posed by the long computing time required for MHD models, physics-based models, which need much shorter computing time, are expected to be used to predict SATs both presently and in the future. We have proposed a physics-based model, called the Shock Propagation Model (SPM), to predict SATs at Earth [*Feng and Zhao*, 2006]. This model combines the analytical solution for the propagation of blast waves from a point source in a moving, steady state, density-variable medium [*Wei*, 1982; *Wei and Dryer*, 1991] with the energy estimation used by the ISPM [*Smith and Dryer*, 1990, 1995]. The input parameters of SPM include the initial shock speed (V_{si}) computed from the Type II radio burst drift rate, the proxy piston-driving time duration (τ), and the background solar wind speed (u_0) detected by L1 spacecraft at the start time of the event. The output of SPM gives the predicted transit time of the shock to any given radial distance R. As an analytical model, SPM can provide prediction results immediately after its input parameters are supplied. Details concerning the SPM can be found in *Feng and Zhao* [2006]. On applying the SPM to 165 solar events during the periods January 1979 to October 1989 and February 1997 to August 2002, it was found that the mean-absolute error of SATs predicted by SPM was about 14 h. This demonstrates that SPM has the capability to be used in the "near real-time" prediction of SATs. However, the SPM presently requires upgrading as follows: (1) The shock strength index at the Earth's location should be introduced into the model in order to predict whether the shock would encounter the Earth; (2) The blast wave theory may not be suitable for all the shocks, since, as pointed out by *Li et al.* [2008], the propagation of some shocks deviates from that of blast waves; (3) The initial speed of the shock wave, as determined by the metric Type II radio burst drift rate, often contains inevitable uncertainty due to the lack of sufficient spatial information concerning radio bursts. All these issues constitute hindrances for the prediction precision of the model. To try to correct or lessen these drawbacks is the objective of this paper, which puts forward an updated version of SPM, called SPM2 hereafter. The paper is organized as follows. In section 2, we give a detailed description of the solar-related-IP shock events used in the present study. Improvements in SPM are described in section 3. In section 4, we present the SPM2, its prediction results, and comparison with other models. A brief summary and discussion is given in section 5.

2. Solar Disturbance-IP Shock Events in Solar Cycle 23

[5] In this study 551 solar-related-IP shock events taken from Fearless Forecast publications are utilized. We selected 168 solar flare-Type II shock events from *Fry et al.* [2003], 151 shock events from *McKenna-Lawlor et al.* [2006], and 232 shock events from *Smith et al.* [2009]. In this way, we collected 551 solar-IP shock events during the period February 1997 to December 2006, covering almost the whole of Solar Cycle 23. *Fry et al.* [2003] listed 173 solar flare-Type II burst events during February 1997 to October 2000, but there are five events among them with $T_{obs} > \frac{1AU}{V_{sw}}$. Here T_{obs} is the observed transit time of the shock from the Sun to the L1 point spacecraft, and V_{sw} is the background solar wind speed. This means that the averaged propagation speed of the shock is lower than the background solar wind speed for these five events. One reason for this could be the spatial variability of V_{sw} (i.e., coronal hole fast wind streams). The relationship between solar disturbances and L1 shocks is "questionable" in these events (called herein questionable events). We thus exclude these five questionable events from our study. *McKenna-Lawlor et al.* [2006] listed 166 solar-IP shock events for the period November 2000 to August 2002 among which is one questionable event ($T_{obs} > \frac{1AU}{V_{sw}}$). In addition, there were 14 shock events associated with more than one solar disturbance in their event list (called herein interaction events), which are excluded from the present study because SPM2 is not designed to take account of shock interactions. *Smith et al.* [2009] presented 245 events during August 2002 to December 2006. This sample contains 13 questionable events ($T_{obs} > \frac{1AU}{V_{sw}}$). For each chosen event, the following parameters are needed: the start time of the Type II burst, the source location of the associated flare, the coronal shock speed computed from the Type II radio burst drift rate, the proxy piston-driving time duration, the background solar wind speed, the arrival time of the associated IP shock at L1 if indeed it arrives, and the prediction results of STOA, ISPM, and HAFv.2 (including whether or not the IP shock could encounter the Earth and when it would arrive if it could arrive). For the total 551 events, only 202 of them had associated IP shocks observed near the Earth, and they are called "with-shock" (abbreviated as "W-shock") events in this paper; the other 349 events were not accompanied at Earth by IP shocks, and they are called "without shock" (abbreviated as "W/O-shock") events. The Fearless Forecast event numbers for these 202 W-shock events, 349 W/O-shock events, 14 interaction events, and 19 (5 + 1 + 13) questionable events are given in Tables S1–S4 in the supporting information, respectively. On applying SPM to the 202 W-shock events in our sample, it was found that the mean-absolute error and root-mean-square error of SATs for these 202 events were 13.19 h and 16.76 h, respectively. As the SPM has no capability to predict whether an IP shock would encounter the Earth, it cannot be used to predict the 349 W/O-shock events.

3. Improvements in the Shock Propagation Model

3.1. Corrections to the Initial Shock Speed

[6] The initial speed of a shock wave is a crucial parameter in predicting the arrival time of the shock. In Fearless

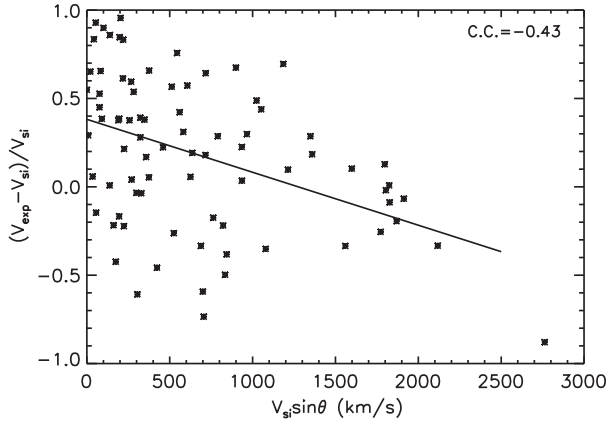

Figure 1. $\frac{V_{exp}-V_{si}}{V_{si}}$ plotted versus $V_{si}\sin\theta$ for 80 events with $|\frac{V_{exp}-V_{si}}{V_{si}}| \leq 1$. V_{exp} is the "expected" initial shock speed by the SPM in order to fit the real arrival time of IP shocks, V_{si} is the coronal shock speed computed from the Type II radio burst drift rate, θ is the source longitude of the shock (determined by the associated flare). The solid line denotes the line fitting to the data points.

Forecast models, this parameter is computed from the frequency drift rate of metric Type II radio bursts, based on an assumed coronal density model, as metric Type II bursts are signatures of coronal shocks. However, the shock speed derived in this way often contains uncertainties since information concerning the propagation direction is not available from solar radio bursts. For example, the radio emission from solar limb located shocks might be generated from the slower portions of the expanding coronal shock so that the fastest part of the shock, while deviating much from the Sun-Earth direction, has only a small surface area exposed to the radio telescope. In this case, the flanks of the shock propagate at some angles to the radial (local vertical) direction. In these circumstances the frequency drift rate and the inferred Type II shock speed will be lower than the actual shock speed [*Fry et al.*, 2003]. *Sun et al.* [2002a, 2002b] pointed out that the initial speed of shock waves, determined by metric Type II radio burst observations, must be substantially reduced (30% on average) for most high-speed shock waves, and adjusting the initial speed can lead to a significant improvement in the SAT prediction accuracy. *Luo et al.* [2011] obtained an empirical formula to adjust the initial shock speed computed from the metric Type II radio burst through comparing simulation results of the HAF model with observations of satellites at 1 AU, namely $\frac{V_{adj}-V_{si}}{V_{si}} = -0.07V_{si}+74$ for the shocks originating in the Western Hemisphere, and $\frac{V_{adj}-V_{si}}{V_{si}} = -0.13V_{si}+124$ for the shocks originating in the Eastern Hemisphere. Here V_{si} is the shock speed computed from the metric Type II radio burst, and V_{adj} is the adjusted shock speed.

[7] Thus, the source location of the shock on the solar surface, especially its longitude, is an important factor influencing the accuracy of the initial shock speed computed from Type II bursts. In this study, we used the SPM to "train" the initial shock speed computed from Type II bursts and developed an empirical method to correct the input V_{si}. Assuming in the first case that we know all the other input parameters as well as the arrival times of these 202 W-shock events except for V_{si}, we used the SPM to derive the "expected" initial shock speed (V_{exp}) for each of them. We then studied the relative difference between the "expected" initial shock speed and the speed computed from the Type II burst drift rate, i.e., $\frac{V_{exp}-V_{si}}{V_{si}}$, and investigated how this relative difference was affected by the Type II burst drift speed V_{si}, duration time τ, source longitude θ, source latitude φ, and their combinations. It was thereby found that $V_{si}\sin\theta$ has the strongest correlation with $\frac{V_{exp}-V_{si}}{V_{si}}$. Figure 1 shows the variation of $\frac{V_{exp}-V_{si}}{V_{si}}$ plotted versus $V_{si}\sin\theta$ for 80 events with $|\frac{V_{exp}-V_{si}}{V_{si}}| \leq 1$. The solid line is the line of fit to the data points, which yields $\frac{V_{exp}-V_{si}}{V_{si}} = 0.3818-3.0\times10^{-4}V_{si}\sin\theta$. Therefore, we obtained the following empirical relation to correct the initial shock speed:

$$V_{si}^{*} = (0.3818 - 3.0\times10^{-4}V_{si}\sin\theta)V_{si} + V_{si} \quad (1)$$

This will be used, see below, in the SPM2 model despite the low correlation coefficient (*C.C.* = –0.43) shown in Figure 1.

3.2. Consideration of Acceleration/Deceleration

[8] After the initial shock speed correction, the prediction of SPM for the 202 W-shock events contains a prediction error $\Delta T = T_{obs} - T_{pred} > 0$ for 114 events, and $\Delta T = T_{obs} - T_{pred} < 0$ for only 88 events. The histogram of event number distribution along ΔT is thus not symmetrical. This means that SPM gives shorter T_{pred} times than those observed (T_{obs}) for the majority of the events ($\Delta T > 0$). A similar result was found by *Li et al.* [2008]. This caused us to add an acceleration/deceleration in term F_{AD} to the shock propagation equation of SPM [*Feng and Zhao*, 2006, equation (7)] in order to remove the distribution asymmetry in these prediction errors (ΔT)

$$V_s = \frac{dR}{dt} = \left[-2\lambda_1 + \sqrt{(2\lambda_1)^2 + \frac{E_0}{J_0 R} + \frac{1}{2J_0}}\right] u_0 \times F_{AD} \quad (2)$$

As the specific form of F_{AD} is not clear, we assumed it to be a constant for each individual shock. The integral of equation (2) gives the predicted arrival time for each shock. The observed arrival times of the 202 W-shock events were used as inputs to solve the integral of equation (2) to

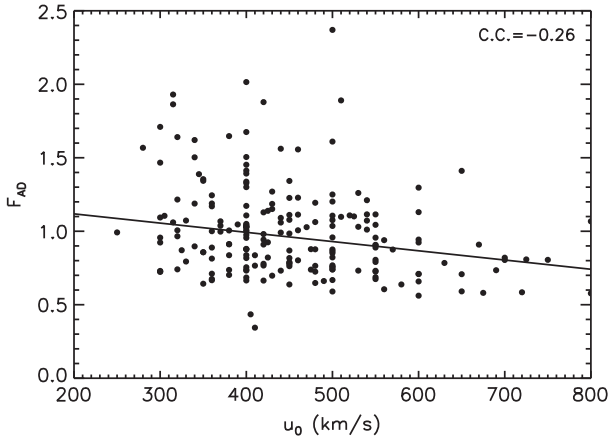

Figure 2. The variation of F_{AD} plotted against the background solar wind speed u_0 for the 202 W-shock events.

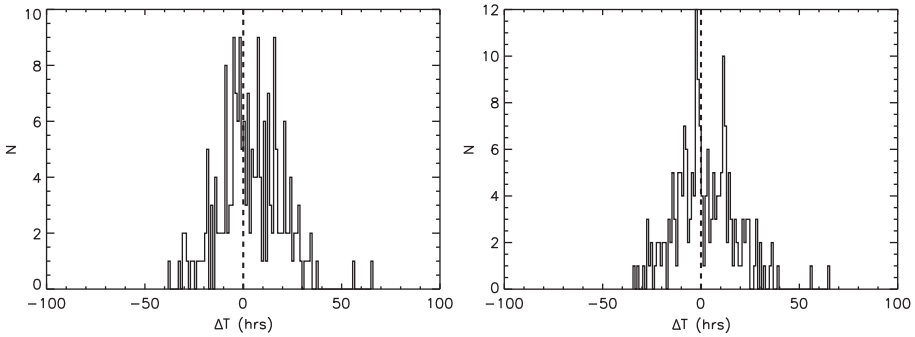

Figure 3. The number frequency distribution of the 202 W-shock events along the prediction error (ΔT) (a) before the acceleration/deceleration correction and (b) after the acceleration/deceleration correction had been applied.

derive F_{AD} for each shock. Then we investigated the correlation between F_{AD} and various input parameters such as V_{si}^{*}, τ, θ, φ, u_0, and possible combinations between them (see section 3.1). It was found that u_0 had the maximum correlation coefficient with F_{AD}. Figure 2 displays the variation of F_{AD} plotted versus u_0 for the 202 W-shock events and the correlation coefficient between them. The line fitting between F_{AD} and u_0 gives

$$F_{AD} = 1.244 - 6.28 \times 10^{-4} u_0 \quad (3)$$

[9] The predictions of equation (2) following the modification provided by equation (3) yields $\Delta T > 0$ for 100 shocks, and $\Delta T < 0$ for 102 shocks. That is, the event numbers for positive and negative errors are nearly equivalent. Therefore, the bias in ΔT is eliminated. Figure 3 shows the number frequency distribution of these 202 W-shock events along ΔT before (Figure 3a) and after (Figure 3b) the corrections provided by equation (3), which clearly indicates this point. Equation (3) reveals that the correction of either acceleration or deceleration depends on the ambient solar wind speed u_0. For high solar wind speed ($u_0 > 388$ km/s), $F_{AD} < 1$ introduces a deceleration correction, while for low solar wind speed ($u_0 < 388$ km/s), $F_{AD} > 1$ involves an acceleration correction.

3.3. Effect of Propagation Direction

[10] According to the blast wave theory adopted in SPM, a shock propagates outward with a circular front. Therefore, the shock will propagate along different directions with the same speed and arrive simultaneously at the same heliodistance. This is definitely not true in real cases. Shocks often propagate with the fastest speed at their "nose" position (i.e., along the main propagation direction) and arrive earlier in this direction than along other directions for the same radial distance. In the STOA model, the shock speed at an angle ψ from the flare radial direction is assumed to be $V_\psi = V_R(1+\cos\psi)/2$, where V_ψ is the blast wave shock front speed at an angle ψ from the flare radial direction and V_R is the wave speed along the flare radial direction. Here to take account of the influence of the shock's propagation direction on its arrival time at Earth, we add a propagation direction term (F_{PD}) in equation (2) as follows:

$$V_s = \frac{dR}{dt} = \left[-2\lambda_1 + \sqrt{(2\lambda_1)^2 + \frac{E_0}{J_0 R} + \frac{1}{2J_0}} \right] u_0 \times F_{AD} \times F_{PD} \quad (4)$$

If it is assumed that the radial direction passing through the Sun center and the source location is the main propagation direction of the IP shock, the direction angle ψ can be computed from $\psi = \arccos(\cos\theta \cos\varphi)$ for the Earth observer, which represents the angular distance between the shock's main propagation direction and the Sun-Earth line. Calculation of F_{PD} and the correlation investigation between F_{PD} and the trigonometric functions of direction angle ψ are carried out in a similar way to what we have done above for F_{AD} in section 3.2. It is found that $\cos\psi$ has the maximum correlation with F_{PD}, as demonstrated in Figure 4. Line fitting to the data points gives

$$F_{PD} = 0.85 + 0.2\cos\psi \quad (5)$$

This correction relation can be used to transform the shock front speed along its main propagation direction to the expected front speed along every direction. Equation (5) also results in a simplified shock front speed profile in three dimensions. An ecliptic plane projection of this shock front speed profile is shown in Figure 5 (solid black line). In this figure we also show for comparison the shock front speed profile adopted by STOA (dotted blue line) and SPM (dashed red line). It can be seen that the shock front speed profile derived here lies between those adopted in STOA and SPM.

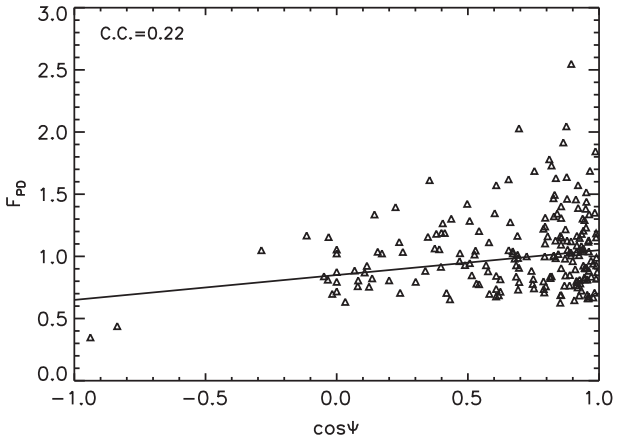

Figure 4. The variation of F_{PD} plotted against $\cos\psi$ for the 202 W-shock events.

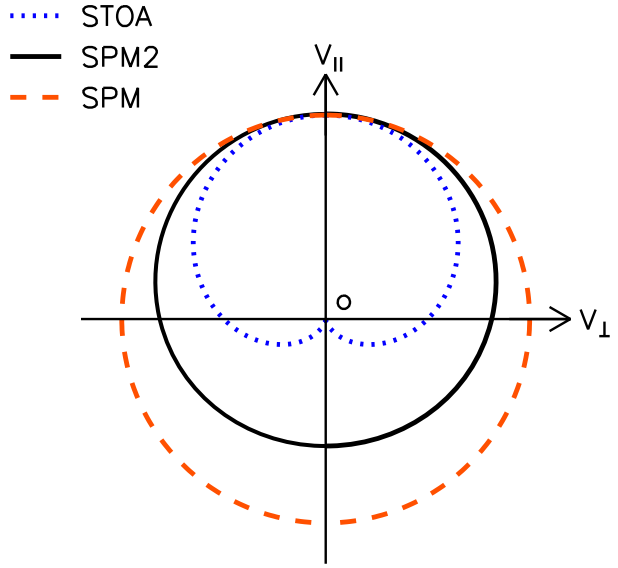

Figure 5. Comparison of the shock front speed profile for STOA (dotted blue line), SPM (dashed red line), and SPM2 (solid black line).

3.4. Equivalent Shock Strength Index

[11] A judgement index is needed to predict whether or not an IP shock will encounter the Earth. The Fearless Forecast models provide ways to estimate the shock strength. STOA uses the shock magnetoacoustic Mach number (M_a) at the Earth's orbit, which is the ratio of the shock speed relative to the characteristic magnetoacoustic speed of plasma in the solar wind frame. Also, the IP shock at Earth is assumed to be a perpendicular shock (the shock normal is perpendicular to the upstream interplanetary magnetic field). A value of $M_a = 1$ is used as the threshold to discriminate the shocks predicted to encounter the Earth from those predicted to decay to MHD waves. In ISPM, a "shock strength index" (SSI, $\log_{10}$ of the ratio of the dynamic pressure jump at the shock relative to the background value) is adopted and the value SSI = 0 is used as a criterion to predict whether an IP shock would encounter the Earth [see *Smith et al.*, 2000]. In HAFv.2, the predicted SATs are extracted from automatic scans of the temporal profiles of the dynamic pressure simulated at L1 using a "shock search index" (SSI_H), i.e., $SSI_H = \Delta P/P_{min}$, where P is either the dynamic pressure or momentum flux, ΔP is the difference in P during consecutive 1 h time steps and P_{min} is the minimum P value for these time steps. $SSI_H = -0.35$ is set as the threshold value for predicting the shock's arrival at Earth. Similar to the Mach number used in STOA, we define the "equivalent shock strength index" (ESSI) as the ratio of the shock speed at the Earth's location relative to the fast-mode wave speed in the frame of solar wind

$$\mathrm{ESSI} = \frac{V_s(\mathrm{EL}) - u_0}{V_f} \tag{6}$$

Here V_s(EL) is the shock speed at the Earth's location predicted by equation (4), and V_f is the fast-mode wave speed of the background solar wind at the Earth's location. In the case of a perpendicular shock, $V_f = \sqrt{V_A^2 + C_s^2}$, where V_A and C_s denote the Alfvén speed and sound speed, respectively. In order to get V_f, the following typical parameters of the solar wind and the interplanetary magnetic field are adopted: $T = 1.5 \times 10^5$ K, $B = 7$ nT, $n = 4.0$ cm^{-3}, $\gamma = 5/3$. These yield $V_f \approx 100$ km/s. For each event in our sample, we can compute its ESSI value through knowing V_s(EL), u_0, and V_f. The next step is to set a threshold value for ESSI, i.e., $\mathrm{ESSI_{tv}}$, to discriminate the shocks that can encounter the Earth from those that cannot. If ESSI $\geq \mathrm{ESSI_{tv}}$, the shock is predicted to encounter the Earth. Otherwise, if ESSI $< \mathrm{ESSI_{tv}}$, the shock is predicted not to encounter the Earth. Figure 6 demonstrates the distribution of the prediction success rates for these two kinds of event along $\mathrm{ESSI_{tv}}$. It can be seen that the prediction success rate for the W-shock events decreases with $\mathrm{ESSI_{tv}}$, while for the W/O-shock events it increases. The two curves intersect at $\mathrm{ESSI_{tv}} = 2.29$, and the prediction success rates are $\sim 61\%$ for both kinds of event. Therefore, we select $\mathrm{ESSI_{tv}} = 2.29$ as the threshold value to predict whether the shock will encounter the Earth to equalize the prediction success rates of both the W-shock and W/O-shock events.

4. SPM2 and Its Prediction Results

4.1. SPM2

[12] Following the corrections introduced in the above indicated steps, a new version of SPM, i.e., SPM2, is established. Input parameters include the initial shock speed (V_{si}) computed from Type II radio bursts, the proxy piston-driving time duration (τ), the angular width of the shock (ω, often assumed to be 60°), the source longitude (θ), source latitude (φ), and the background solar wind speed (u_0). These inputs are used to compute the propagation speed of the shock at the Earth's location (V_s(EL)) according to

$$V_s = \frac{\mathrm{d}R}{\mathrm{d}t} = \left[-2\lambda_1 + \sqrt{(2\lambda_1)^2 + \frac{E_0}{J_0 R} + \frac{1}{2J_0}}\right] u_0 \times F_{\mathrm{AD}} \times F_{\mathrm{PD}} \tag{7}$$

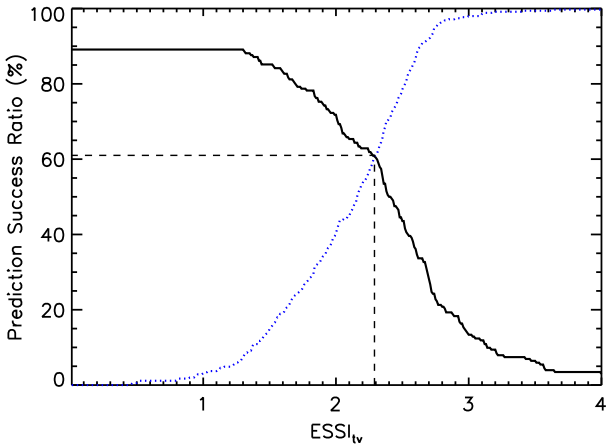

Figure 6. The prediction success rate for the W-shock events (solid black line) and W/O-shock events (dotted blue line) plotted versus the threshold values of ESSI that were used to predict whether or not a shock would encounter the Earth. The coordinates for the intersection point of the two curves are indicated by the vertical dashed line and the horizontal dashed line.

Table 1. Forecast Contingency Table of Hits, Misses, False Alarms, and Correct Nulls for the Prediction Results of SPM2 and HAFv.2 for 551 Events of Solar Cycle 23 (February 1997 to December 2006)[a]

	Forecast		SPM2 Prediction		HAFv.2 Prediction	
Observation	Yes	No	Yes	No	Yes	No
Yes	a	c	123	79	154	48
No	b	d	137	212	207	142
Total	a + b	c + d	260	291	361	190

[a]Definitions and explanations: a = Hits, b = False alarm, c = Miss, d = Correct null. This table is transposed from the format adopted by *Smith et al.* [2000], *Fry et al.* [2001, 2003], and *McKenna-Lawlor et al.* [2006] in order to facilitate comparisons of these models.

Here $E_0 = \frac{C.V_{si}^{*3}.\omega.(\tau+D)}{Au_0^2}$, $V_{si}^* = (0.3818 - 3.0\times10^{-4}V_{si}\sin\theta)V_{si} + V_{si}$, $F_{AD} = 1.244 - 6.28\times10^{-4}u_0$, $F_{PD} = 0.85 + 0.2\cos\theta\cos\varphi$, A = 300 kg m^{-1}, C = 0.283 × 10^{20}erg.m^{-3}. sec^{-2}.deg^{-1}, and D = 0.52 h. Then, the "equivalent shock strength index" (ESSI) for each event is derived to be

$$\mathrm{ESSI} = \frac{V_s(\mathrm{EL}) - u_0}{V_f} \tag{8}$$

with $V_f \approx 100$ km/s. If ESSI $\geq$ ESSI$_{tv}$ = 2.29, the shock is predicted to encounter the Earth. Otherwise, if ESSI < ESSI$_{tv}$ = 2.29, the shock is predicted to miss the Earth. For the events with ESSI $\geq$ ESSI$_{tv}$ = 2.29, the following equation is used to predict shock arrival times at Earth:

$$T = \frac{J_0}{u_0\times F_{AD}\times F_{PD}}\left\{ 4\lambda_1[R + 2E_0 - 2E_0\ln(R+2E_0)] + 2\sqrt{X} - \frac{(16\lambda_1^2+\frac{1}{J_0})E_0}{\sqrt{4\lambda_1^2+\frac{1}{2J_0}}}\times\ln\left[\sqrt{X} + (R+2E_0)\sqrt{4\lambda_1^2+\frac{1}{2J_0}} - \frac{\left(16\lambda_1^2+\frac{1}{J_0}\right)E_0}{2\sqrt{4\lambda_1^2+\frac{1}{2J_0}}}\right] - 8\lambda_1E_0\times\ln\left[\frac{\sqrt{X}+4\lambda_1E_0}{(R+2E_0)} - \frac{\left(16\lambda_1^2\frac{1}{J_0}\right)}{8\lambda_1}\right]\right\} + T_0 \tag{9}$$

with $\sqrt{X} = \sqrt{\frac{E_0}{J_0}R + (\frac{1}{2J_0})R^2}$, R = 1 AU, and T_0 is determined by the restriction $R = 0$ when $T = 0$.

Table 2. Forecast Contingency Table of Hits, Misses, False Alarms, and Correct Nulls for the Prediction Results of SPM2 and STOA for 463 Events That STOA Has Predictions For[a]

	Forecast		SPM2 Prediction		STOA Prediction	
Observation	Yes	No	Yes	No	Yes	No
Yes	a	c	106	61	133	34
No	b	d	113	183	186	110
Total	a + b	c + d	219	244	319	144

[a]Definitions and explanations: the same as Table 1.

4.2. Prediction Results, Verification, and Statistics

[13] The 2 × 2 "contingency table" is often used in the evaluation of meteorological models [e.g., *Schaefer*, 1990]. It provides information about the success or failure of the forecast in the data set and has been employed in Fearless Forecast models [*Fry et al.*, 2003; *McKenna-Lawlor et al.*, 2006, 2012; *Smith et al.*, 2009]. In this paper, we follow the fundamental definitions adopted in the Fearless Forecasts, namely, if a shock is predicted to arrive and actually observed within ± 24 h, then the prediction is called a "Hit" (h); if a shock is detected, but predicted not to arrive, or predicted to arrive 24 h away from the detection time, this prediction is called a "Miss" (m); if a shock is predicted to arrive, but no shock is observed 1–5 days after the solar event, then the prediction is called a "False alarm" (fa); and if a shock is neither predicted to arrive nor detected 1–5 days after the solar event, then this prediction is called a "Correct null" (cn). These definitions are used to divide the solar events of our sample into hits, misses, false alarms, and correct nulls according to the prediction results. The predictions of SPM2 for 551 sample events yielded 123 hits, 137 false alarms, 79 misses, and 212 correct nulls. Table 1 demonstrates the forecast 2 × 2 contingency table for the prediction results of SPM2 and HAFv.2. In this table, a, b, c, and d denote the number of hits, false alarms, misses, and correct nulls, respectively. N = a + b + c + d stands for the total event number, which is 551 for SPM2 and HAFv.2. This table is transposed from the format adopted by *Smith et al.* [2000] and *Fry et al.* [2001, 2003] to list the prediction results of SPM2 and HAFv.2 side by side. Similarly, Tables 2 and 3 give the forecast 2 × 2 contingency table to compare the prediction results of SPM2 with those of STOA and ISPM based on rather similar data sets, which are 463 events for STOA and 418 events for ISPM (see http://www2.gi.alaska.edu/pipermail/gse-ff/).

[14] A range of statistical forecast skill scores can be computed from the contingency table in order to evaluate the model's prediction result. These skill scores include (1) probability of detection, yes, PODy = a/(a + c); (2) probability of detection, no, PODn = d/(b + d); (3) false alarm ratio, FAR = b/(a + b); (4) bias, BIAS = (a + b)/(a + c); (5) critical success index, CSI = a/(a + b + c); (6) true skill statistic, TSS = PODy + PODn – 1; (7) Heidke skill score, HSS = (a + d – C1)/(N – C1), here C1 = C2 + (b + d)(c + d)/N, C2 = (a + c)(a + b)/N; (8) Gilbert skill score, GSS = (a – C2)/(a + b + c – C2); (9) success rate, SR = (a + d)/N. Details about the definitions and applications of these skill scores can be found in *Schaefer* [1990], *Mozer and Briggs* [2003], *Smith et al.* [2009], and *McKenna-Lawlor et al.*

Table 3. Forecast Contingency Table of Hits, Misses, False Alarms, and Correct Nulls for the Prediction Results of SPM2 and ISPM for 418 Events That ISPM Has Predictions For[a]

	Forecast		SPM2 Prediction		ISPM Prediction	
Observation	Yes	No	Yes	No	Yes	No
Yes	a	c	97	55	78	74
No	b	d	103	163	98	168
Total	a + b	c + d	200	218	176	242

[a]Definitions and explanations: the same as Table 1.

Table 4. Statistical Comparison of the Values of Several Standard Meteorological Forecast Skill Scores Derived by SPM2 With Those Derived by HAFv.2, STOA and ISPM Based on Rather Similar Data Sets of Solar Cycle 23 (February 1997 to December 2006)[a]

Forecast skill score	SPM2	HAFv.2	SPM2	STOA	SPM2	ISPM
Probability of detection, yes (PODy)	0.61	0.76	0.64	0.80	0.64	0.51
Probability of detection, no (PODn)	0.61	0.41	0.62	0.37	0.61	0.63
False alarm ratio (FAR)	0.53	0.57	0.52	0.58	0.52	0.56
BIAS	1.29	1.79	1.31	1.91	1.32	1.16
Critical success index (CSI)	0.36	0.38	0.38	0.38	0.38	0.31
True skill statistic (TSS)	0.22	0.17	0.25	0.17	0.25	0.15
Heidke skill score (HSS)	0.20	0.15	0.24	0.14	0.24	0.14
Gilbert skill score (GSS)	0.11	0.08	0.13	0.08	0.13	0.08
Success Rate (SR)	0.61	0.54	0.62	0.53	0.62	0.59
χ^2	24.0	16.2	27.4	14.1	24.4	8.3
p_3	9.5×10^{-7}	5.6×10^{-5}	1.7×10^{-7}	1.8×10^{-4}	7.8×10^{-7}	0.0039

[a]The Event Number of Similar Data Sets Is 551 for HAFv.2, 463 for STOA, and 418 for ISPM.

[2012]. The specific parameter of interest to a user depends on his/her purpose. For example, if a user is interested in the prediction success rate of the observed shocks, then PODy (the ratio between the shocks correctly predicted and all the shocks observed) is the crucial parameter. A value 1 of PODy means that all the observed shocks are correctly predicted. Therefore, 1 is called here the "ideal value" of PODy. Similarly, PODn compares the number of correct nulls to that of false alarms, and PODn=1 means that all the nonshock events are predicted not to encounter the Earth. SR gives the prediction success rate for the combined shock and nonshock events. However, it should be pointed out that among these various standard parameters, only PODn, TSS, HSS, and SR involve correct nulls. These forecast skill scores have earlier been used to evaluate the Fearless Forecast models [e.g., *Fry et al.*, 2003; *McKenna-Lawlor et al.*, 2006, 2012; *Smith et al.*, 2009]. Table 4 gives a statistical comparison of these skill scores derived by SPM2 with those derived by HAFv.2 based on 551 rather similar events, with those by STOA on 463 events, and with those by ISPM on 418 events. The prediction success rate of SPM2 is 0.61 for both the W-shock events (PODy) and W/O-shock events (PODn). Although HAFv.2 with PODy being 0.76 performs better than SPM2 for the W-shock events, it performs worse for the W/O-shock events (with PODn being only 0.41). The prediction success rate of SPM2 is slightly higher (SR = 0.61) than that of HAFv.2 (SR = 0.54) for the total 551 events. It should be noted that *McKenna-Lawlor et al.* [2012] showed for a sample of 584 events that the parameter PODy yielded values for the rise/maximum/decay phases of Solar Cycle 23 and when using the composite sample of 0.85, 0.64, 0.79, and 0.77. Also, that the parameters SR obtained were correspondingly only 0.53, 0.51, 0.59, and 0.55. McKenna-Lawlor's analysis provided evidence as to how changing circumstances on the Sun and in interplanetary space can affect the performance of the HAFv.2 model. The effect of solar cycle phase on the model's performance and corresponding comparisons between different models will not be taken into account in the present paper but will be considered in our future work. For all nine forecast skill scores from PODy to SR (row 2 to row 10 in Table 4), PODn, FAR, BIAS, TSS, HSS, GSS, and SR of SPM2 yield better values than those of HAFv.2, but the values of PODy, CSI of SPM2 are worse than those of HAFv.2. A χ^2 test was also used to validate the model's prediction capability as demonstrated in rows 11 and 12 of Table 4. Here the p-value is estimated for 3 degrees of freedom, and a value of $p_3 < 0.05$ indicates a high level of significance [*McKenna-Lawlor et al.*, 2012]. Higher values of χ^2 and lower values of p_3 mean that the dependence between observations and predictions is stronger. The p_3 values of both SPM2 and HAFv.2 are less than 0.05. This indicates a high level of significance for their predictions. Similarly, the values of PODn, FAR, BIAS, TSS, HSS, GSS, and SR of SPM2 are better than those of STOA, and the values of PODy, FAR, CSI, TSS, HSS, GSS, and SR of SPM2 are better than those of ISPM for the data samples compared. Also, the χ^2 tests demonstrate that SPM2 has the highest prediction performance.

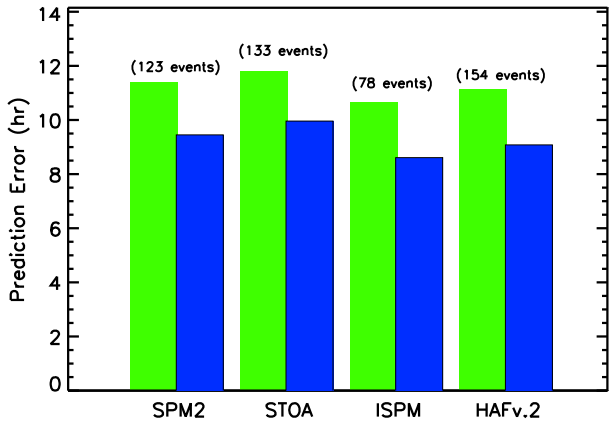

Figure 7. Comparisons of the prediction error of SPM2, STOA, ISPM, and HAFv.2 models: the root-mean-square (RMS) ΔT (green bars) and the mean-absolute ΔT (blue bars). The number of "hit" shocks for each model is labeled on top of the bars.

[15] The prediction error ΔT, i.e., the difference between the observed and predicted arrival times is another parameter used to demonstrate the prediction precision of models. The root-mean-square (RMS) and mean-absolute value are two commonly used measurements of ΔT. The RMS ΔT of SPM2 is 11.39 h for 123 "hit" shocks. Similarly, the RMS ΔT of STOA, ISPM, and HAFv.2 are 11.79 h for 133 "hit" shocks, 10.68 h for 78 "hit" shocks, and 11.14 h for 154 "hit" shocks, respectively. The mean-absolute ΔT of the four models range from 8.6 h to 10.0 h, while this error of SPM2

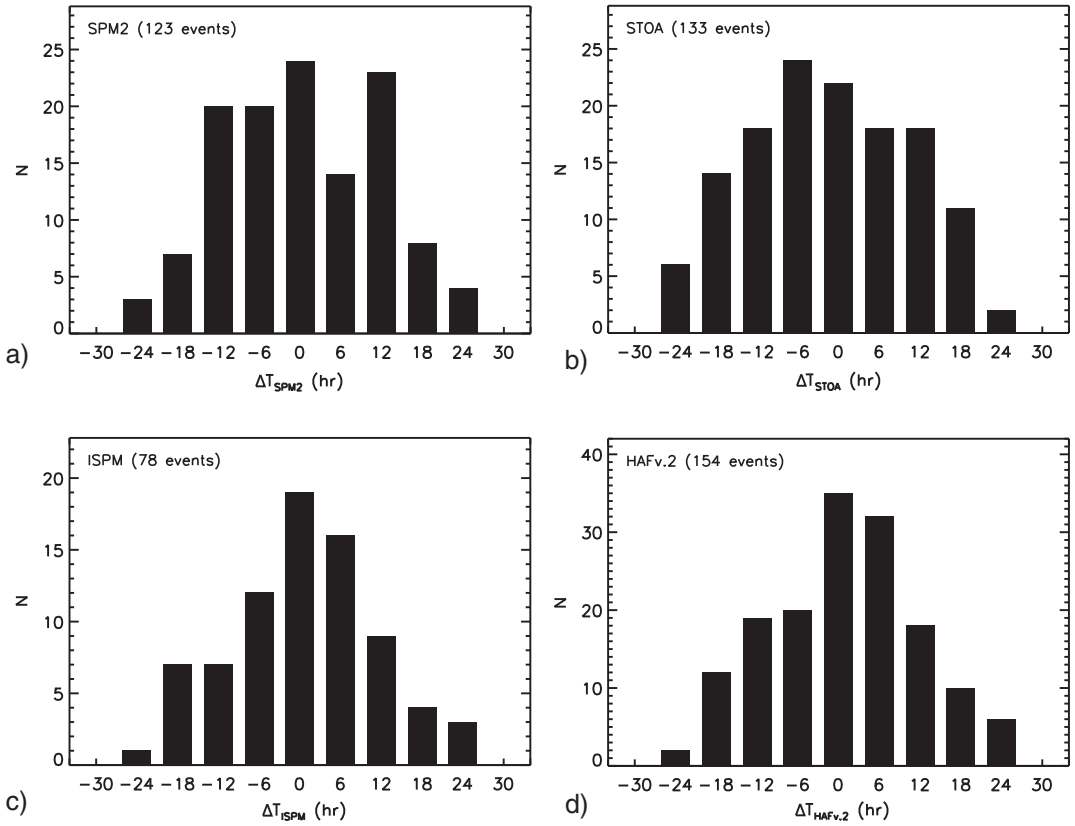

Figure 8. Histograms showing the arrival time error (ΔT) between the observed and predicted values for the models (a) SPM2, (b) STOA, (c) ISPM, and (d) HAFv.2. The number of "hit" shocks registered by each model is entered on.

is 9.45 h. Figure 7 displays the comparison of the prediction error of four models for their "hit" shocks. Green bars in this figure denote the RMS error, and blue bars denote the mean-absolute error. The number of "hit" shocks for each model is also shown on top of the bar. Figure 8 gives for SPM2, STOA, ISPM, and HAFv.2 the histograms of ΔT for their "hit" shocks. For each model, the event number is highest near the zero-error location and decreases with increasing $|\Delta T|$. This property showing an approximately normal distribution in ΔT demonstrates the reasonableness and rationality of the model's prediction.

5. Conclusion and Discussion

[16] On the basis of the Shock Propagation Model (SPM), a series of corrections and improvements are adopted in this paper to improve the performance of SPM. These corrections comprise adjusting the initial shock speed computed from the Type II radio burst drift rate, adding an acceleration/deceleration term in the propagation function of blast waves, considering the effect of the shock's propagation direction on its arrival time, and defining the equivalent shock strength index (ESSI) as the judging parameter to predict whether a shock will encounter the Earth. These efforts lead to a new version of the model, i.e., SPM2. In order to check the prediction efficiency of SPM2, 551 solar-IP shock events in Solar Cycle 23 were utilized to train the performance of SPM2. The prediction results demonstrate that the prediction success rate of $\sim$ 60% for SPM2 and the values for some skill scores are a little higher than those attained using the Fearless Forecast models. Variations due to the solar cycle phase are not taken into account in these estimations. For the prediction error of SATs, the RMS error is within 12 h with the mean-absolute error within 10 h, respectively. Especially, SPM2 can provide predictions immediately given the input parameters. All of these results demonstrate the value of SPM2 as a real-time space weather prediction tool.

[17] The superiority of SPM2 in contrast to SPM is due to the combined effect of four correction steps. As far as each step is concerned, the correction is empirical and limited. For example, only 80 events with $|\frac{V_{\rm exp}-V_{\rm si}}{V_{\rm si}}| \leq 1$ were used to derive the empirical relation of adjusting the initial shock speed, instead of utilizing all the 202 W-shock events. This is because $V_{\rm exp} < 0$, or $V_{\rm exp} - V_{\rm si} > V_{\rm si}$ for the remaining 122 events. Inclusion of these 122 events would make the relation between $\frac{V_{\rm exp}-V_{\rm si}}{V_{\rm si}}$ and $V_{\rm si}\sin\theta$ more complicated. Especially, *Sun et al.* [2002a, 2002b] found similar relations between the initial speed provided by metric Type II radio bursts and an ex post facto "adjusted speed". The mean-absolute error of ΔT for the 202 events was reduced from 13.19 h to 12.81 h after this correction step. In the correction of acceleration/deceleration, our aim was to equalize the event numbers of $\Delta T > 0$ and $\Delta T < 0$, and additionally, the mean-absolute error showed a decrease of 0.55 h (from 12.81 h to 12.26 h). The consideration of propagation direction only produced a decrease of 0.22 h in the mean-absolute error (from 12.26 h to 12.04 h), while the RMS error

is decreased by 0.57 h (from 15.84 h to 15.27 h). This may imply that the arrival time of a shock does not depend significantly on its propagation direction as being anticipated. The adoption of ESSI strengthens the predictive ability of SPM2 as to whether a shock will encounter the Earth. But the threshold value ($ESSI_{tv}$) is set to be 2.29, rather than the theoretical value 1 in order to equalize the prediction success rates of the W-shock and W/O-shock events. If $ESSI_{tv} = 1$ is adopted, then the prediction success rate for the W-shock events is raised to nearly 90%, but for the W/O-shock events it is decreased below 5% as demonstrated in Figure 6. Similarly, STOASEP used $M_a \geq 2$ directly to predict that the shock would encounter the Earth no matter whether the SEP was detected or not [*Qin et al.*, 2009]. In addition, the classification of those events with $|\Delta T| \geq 24$ in the "Miss" catalogue in section 4.2 decreased the prediction error greatly (the mean-absolute error decreased from 12.04 h to 9.45 h; the RMS error decreased from 15.27 h to 11.39 h).

[18] It should be mentioned that SPM2 does not take into account the influence of the structured solar wind on the shock's propagation in the IP medium, such as coronal density inhomogeneities, fluctuations, high speed solar wind, heliospheric current sheet, and their combinations. These structures would have evident effects on the shock's propagation and corresponding arrival time at Earth as pointed out by other researchers [e.g., *Heinemann*, 2002; *Feng and Zhao*, 2006; *Wu et al.*, 2006]. Especially, the interactions of two or more shocks in IP space are missed in the SPM2 model. This kind of interaction can lead to a situation where more than one solar disturbance is related to one IP shock in the Earth space. On the other hand, a blast wave may not be suitable to represent the shock wave driven by the Interplanetary Coronal Mass Ejection (ICME) all the way from the Sun to 1 AU [*Leblanc et al.*, 2001]. Further improvement of SPM2 at hand will be the solar cycle phase effect and verification by new events from Solar Cycle 24.

[19] **Acknowledgments.** This work is jointly supported by the National Basic Research Program (973 program) under grant 2012CB825601, the Knowledge Innovation Program of the Chinese Academy of Sciences (KZZD-EW-01-4), the National Natural Science Foundation of China (41031066, 41231068, 41274179, 41274192, 41074121, 41074122, and 40904048), and the Specialized Research Fund for State Key Laboratories. We thank the Fearless Forecast papers and their website for providing the event list. We also thank Gang Qin and Huilian Liu for the χ^2 test program that they provided as well as beneficial discussions with them. Special thanks go to the referee for his/her very good suggestions to the improvement of the manuscript.

[20] Philippa Browning thanks the reviewers for their assistance in evaluating this paper.

References

Dryer, M., and D. F. Smart (1984), Dynamical models of coronal transients and interplanetary disturbances, *Adv. Space Res.*, *4*, 291–301.

Dryer, M., C. D. Fry, W. Sun, C. S. Deehr, Z. Smith, S.-I. Akasofu, and M. D. Andrews (2001), Prediction in real-time of the 2000 July 14 heliospheric shock wave and its companions during the "Bastille" epoch, *Sol. Phys.*, *204*, 265–284.

Dryer, M., Z. Smith, C. D. Fry, W. Sun, C. S. Deehr, and S.-I. Akasofu (2004), Real-time shock arrival predictions during the "Halloween 2003 epoch", *Space Weather*, *2*, S09001, doi:10.1029/2004SW000087.

Feng, X. S., and X. H. Zhao (2006), A new prediction method for the arrival time of interplanetary shocks, *Sol. Phys.*, *238*, 167–186.

Feng, X. S., Y. F. Zhou, and S. T. Wu (2007), A novel numerical implementation for solar wind modeling by the modified conservation element/solution element method, *Astrophys. J.*, *655*, 1110–1126.

Feng, X. S., Y. Zhang, W. Sun, M. Dryer, C. D. Fry, and C. S. Deehr (2009a), A practical database method for predicting arrivals of "average" interplanetary shocks at Earth, *J. Geophys. Res.*, *114*, A01101, doi:10.1029/2008JA013499.

Feng, X. S., Y. Zhang, L. P. Yang, S. T. Wu, and M. Dryer (2009b), An operational method for shock arrival time prediction by one-dimensional CESE-HD solar wind model, *J. Geophys. Res.*, *114*, A10103, doi:10.1029/2009JA014385.

Feng, X. S., L. P. Yamg, C. Q. Xiang, S. T. Wu, Y. F. Zhou, and D. K. Zhong (2010), Three-dimensional solar wind modeling from the Sun to Earth by a SIP-CESE MHD model with a six-component grid, *Astrophys. J.*, *723*, 300–319.

Feng, X. S., S. Zhang, C. Zhang, L. Yang, C. Jiang, and S. T. Wu (2011), A hybrid solar wind model of the CESE+HLL method with a Yin-Yang overset grid and an AMR grid, *Astrophys. J.*, *734*, 50, doi:10.1088/0004-637X/734/1/50.

Feng, X. S., L. P. Yang, C. Q. Xiang, C. W. Jiang, X. P. Ma, S. T. Wu, D. K. Zhong, and Y. F. Zhou (2012a), Validation of the 3D AMR SIP-CESE solar wind model for four Carrington rotations, *Sol. Phys.*, *279*, 207–229.

Feng, X. S., C. W. Jiang, C. Q. Xiang, X. P. Zhao, and S. T. Wu (2012b), A data-driven model for the global coronal evolution, *Astrophys. J.*, *758*, 62, doi:10.1088/0004-637X/758/1/62.

Fry, C. D., W. Sun, C. S. Deehr, M. Dryer, Z. Smith, S.-I. Akasofu, M. Tokumaru, and M. Kojima (2001), Improvements to the HAF solar wind model for space weather predictions, *J. Geophys. Res.*, *106*, 20,985–21,001.

Fry, C. D., M. Dryer, Z. Smith, W. Sun, C. S. Deehr, and S.-I. Akasofu (2003), Forecasting solar wind structures and shock arrival times using an ensemble of models, *J. Geophys. Res.*, *108*, 1070, doi:10.1029/2002JA009474.

Fry, C. D., T. R. Detman, M. Dryer, Z. Smith, W. Sun, C. S. Deehr, S.-I. Akasofu, C.-C. Wu, and S. McKenna-Lawlor (2007), Real time solar wind forecasting: Capabilities and challenges, *J. Atmos. Solar Terr. Phys.*, *69*, 109–115.

Heinemann, M. (2002), Effects of solar wind inhomogeneities on transit times of interplanetary shock waves, *J. Atmos. Terr. Phys.*, *64*, 315–325.

Leblanc, Y., G. A. Dulk, A. Vourlidas, and J.-L. Bougeret (2001), Tracing shock waves from the corona to 1 AU: Type II radio emission and relationship with CMEs, *J. Geophys. Res.*, *160*, 25,301–25,312.

Li, H. J., F. S. Wei, X. S. Feng, and Y. Q. Xie (2008), On improvement to the Shock Propagation Model (SPM) applied to interplanetary shock transit time forecasting, *J. Geophys. Res.*, *113*, A09101, doi:10.1029/2008JA013167.

Liu, H.-L., and G. Qin (2012), Using soft X-ray observations to help the prediction of flare related interplanetary shocks arrival times at the Earth, *J. Geophys. Res.*, *117*, A04108, doi:10.1029/2011JA017220.

Luo, H., G. X. Chen, A. M. Du, W. Sun, W. Y. Xu, Y. Zhang, X. D. Zhao, and Y. Wang (2011), Influence of the initial shock speed excited by solar flares on shock arrival time prediction, *Chinses J. Geophys.*, *54*, 1945–1952.

McKenna-Lawlor, S. M. P., M. Dryer, Z. Smith, K. Kecskemety, C. D. Fry, W. Sun, C. S. Deehr, D. Berdichevsky, K. Kudela, and G. Zastenker (2002), Arrival times of flare/halo CME associated shocks at the Earth: Comparison of the predictions of three numerical models with these observations, *Ann. Geophys.*, *20*, 917–935.

McKenna-Lawlor, S. M. P., M. Dryer, M. D. Kartalev, Z. Smith, C. D. Fry, W. Sun, C. S. Deehr, K. Kecskemety, and K. Kudela (2006), Near real-time predictions of the arrival at Earth of flarerelated shocks during Solar Cycle 23, *J. Geophys. Res.*, *111*, A11103, doi:10.1029/2005JA011162.

McKenna-Lawlor, S. M. P., C. D. Fry, M. Dryer, D. Heynderickx, K. Kecskemety, K. Kudela, and J. Balaz (2012), A statistical study of the performance of the Hakamada-Adasofu-Fry version 2 numerical model in predicting solar shock arrival times at Earth during different phases of solar cycle 23, *Ann. Geophys.*, *30*, 405–419.

Mozer, J. B., and W. M. Briggs (2003), Skill in real-time solar wind shock forecasts, *J. Geophys. Res.*, *108*(A6), 1262, doi:10.1029/2003JA009827.

Qin, G., M. Zhang, and H. K. Rassoul (2009), Prediction of the shock arrival time with SEP observations, *J. Geophys. Res.*, *114*, A09104, doi:10.1029/2009JA014332.

Russell, C. T., et al. (2000), The interplanetary shock of September 24, 1998: Arrival at Earth, *J. Geophys. Res.*, *105*, 25,143–25,154.

Schaefer, J. T. (1990), Critical success index as an indication of warning skill, *Weather Forecast.*, *3*, 570–575.

Smart, D. F., and M. A. Shea (1984), A simplified technique for estimating the arrival time of solar flare–initiated shocks, in *Proceedings of STIP Workshop on Solar/Interplanetary Intervals*, edited by M. A. Shea, D. F. Smart, and S. McKenna-Lawlor, pp. 139–256, Book Crafters, Chelsea, Mich.

Smart, D. F., and M. A. Shea (1985), A simplified model for timing the arrival of solar flare-initiated shocks, *J. Geophys. Res.*, *90*, 183–190.

Smith, Z., and M. Dryer (1990), MHD study of temporal and spatial evolution of simulated interplanetary shocks in the ecliptic plane within 1AU, *Sol. Phys.*, *129*, 387–405.

Smith, Z., and M. Dryer (1995), The interplanetary Shock Propagation Model: A model for predicting solar-flare-caused geomagnetic storms, based on the 2 1/2D, MHD numerical simulation results from the interplanetary global model, *NOAA Tech. Memo. ERL SEL-89*, *123*, 453–470.

Smith, Z., M. Dryer, E. Ort, and W. Murtagh (2000), Performance of interplanetary shock prediction models: STOA and ISPM, *J. Atmos. Solar Terr. Phys.*, *62*, 1265–1274.

Smith, Z., M. Dryer, and C. D. Fry (2005), Determining shock velocities for inputs to Sun-to-Earth models from radio and coronagraph data, *Space Weather*, *3*, S07002, doi:10.1029/2004SW000136.

Smith, Z. K., M. Dryer, S. M. P. McKenna-Lawlor, C. D. Fry, C. S. Deehr, and W. Sun (2009), Operational validation of HAFv2's predictions of interplanetary shock arrivals at Earth: Declining phase of Solar Cycle 23, *J. Geophys. Res.*, *114*, A05106, doi:10.1029/2008JA013836.

Sun, W., M. Dryer, C. D. Fry, C. S. Deehr, Z. Smith, S.-I. Akasofu, M. D. Kartalev, and K. G. Grigorov (2002a), Evaluation of solar Type II radio burst estimates of initial solar wind shock speed using a kinematic model of the solar wind on the April 2001 solar wind swarm, *Geophys. Res. Lett.*, *29*, 1171, doi:10.1029/2001GL013659.

Sun, W., M. Dryer, C. D. Fry, C. S. Deehr, Z. Smith, S.-I. Akasofu, M. D. Kartalev, and K. G. Grigorov (2002b), Real-time forecasting of ICME shock arrivals at L1 during the "April Fools Day" epoch: 28 March–21 April 2001, *Ann. Geophys.*, *20*, 937–945.

Sun, W., C. S. Deehr, C. D. Fry, M. Dryer, Z. Smith, and S.-I. Akasofu (2003), Plane-of-sky simulations of interplanetary shock waves, *Geophys. Res. Lett.*, *30*, 2044, doi:10.1029/2003GL017574.

Wei, F. S. (1982), The blast wave propagating in a moving medium variable density, *Chinese J. Space Sci.*, *2*(1), 63–72.

Wei, F. S., and M. Dryer (1991), Propagation of solar flare-associated interplanetary shock waves in the heliospheric meridional plane, *Sol. Phys.*, *132*, 373–394.

Wu, C.-C., X. S. Feng, S. T. Wu, M. Dryer, and C. D. Fry (2006), Effects of the interaction and evolution of interplanetary shocks on "background" solar wind speeds, *J. Geophys. Res.*, *111*, A12104, doi:10.1029/2006JA011615.

Zhou, Y. F., X. S. Feng, S. T. Wu, D. Du, F. Shen, and C. Q. Xiang (2012), Using a 3-D spherical plasmoid to interpret the Sun-to-Earth propagation of the 4 November 1997 coronal mass ejection event, *J. Geophys. Res.*, *117*, A01102, doi:10.1029/2010JA016380.